PHYSICAL REVIEW FLUIDS **2**, 072601(R) (2017)

Turbulence intermittency in a multiple-time-scale Navier-Stokes-based reduced model

Perry L. Johnson* and Charles Meneveau

Department of Mechanical Engineering and Center for Environmental and Applied Fluid Mechanics, Johns Hopkins University, 3400 North Charles Street, Baltimore, Maryland 21218, USA

(Received 29 March 2017; published 28 July 2017; corrected 29 January 2018)

Intermittency of small-scale motions is an ubiquitous facet of turbulent flows, and predicting this phenomenon based on reduced models derived from first principles remains an important open problem. Here, a multiple-time-scale stochastic model is introduced for the Lagrangian evolution of the full velocity gradient tensor in fluid turbulence at arbitrarily high Reynolds numbers. Unlike previous phenomenological models of intermittency, in the proposed model the dynamics driving the growth of intermittency due to gradient self-stretching and rotation are derived directly from the Navier-Stokes equations. Numerical solutions of the resulting set of stochastic differential equations show that the model predicts anomalous scaling for moments of the velocity gradient components and negative derivative skewness. It also predicts signature topological features of the velocity gradient tensor such as vorticity alignment trends with the eigen directions of the strain rate.

DOI: 10.1103/PhysRevFluids.2.072601

The phenomenon of small-scale intermittency, universal across a wide range of turbulent flows [1], represents a long-standing challenge to developing a theory for fluid turbulence that is based on first principles, i.e., derivable from the Navier-Stokes equations [2–5]. The manifestation of intermittency is that fluctuations in velocity gradients or increments become more extreme and violent [6,7], exhibiting longer (fatter) tails in their probability distribution, with increasing Reynolds number or shrinking observation length scale. Such extreme events can affect phenomena ranging from flame extinction, droplet breakup, and heavy particle clustering in turbulent flows.

The refined similarity hypotheses [2,3] and the multifractal formalism [4,8,9] have provided a conceptual framework for understanding intermittency, and various types of phenomenological descriptions such as cascade models [4,9,10], shell models [11], and stochastic Markov processes for velocity increments across scales [12] have been constructed to be consistent with the energy cascading mechanism. Using adjustable parameters, these models can describe empirical intermittency exponents. However, connecting these models and their intermittency exponents with the incompressible Navier-Stokes equations through a systematic derivation has proved to be an elusive goal. The only *ab initio* intermittency prediction is for the Kraichnan model for passive scalars in a random (prescribed) velocity field [13].

Intermittency at the small scales of turbulence can be described using the scaling of velocity gradient moments with Reynolds number, such as $\langle|\partial u/\partial x|^m\rangle \sim (\langle\epsilon\rangle/\nu)^{m/2}\mathrm{Re}_\lambda^{\alpha(m)}$, where $\mathrm{Re}_\lambda = \sqrt{15}u'^2/\sqrt{\nu\langle\epsilon\rangle}$ is the Taylor-scale Reynolds number, u' is the turbulent root-mean-square velocity (turbulent kinetic energy is $\frac{3}{2}u'^2$), ν is the fluid's kinematic viscosity, and $\langle\epsilon\rangle$ is the flow's mean dissipation rate. Intermittency can be observed as deviations from $\alpha(m) = 0$. We remark that Re_λ represents a ratio of time scales between the slowest and fastest motions of the turbulent flow, $\mathrm{Re}_\lambda \sim T/\tau_K$, where $T \sim u'^2/\langle\epsilon\rangle$ is the large-eddy turnover time and $\tau_K = \sqrt{\nu/\langle\epsilon\rangle}$ is the Kolmogorov time [14].

*pjohns86@jhu.edu

The velocity gradient tensor, $A_{ij} = \partial u_i/\partial x_j$, encompasses both the strain rate (local deformation rate) and vorticity (local rotation rate), providing a rich quantitative description of the local flow conditions. The gradient of the Navier-Stokes equations for incompressible flow reads

$$\frac{d}{dt}A_{ij} = -\left(A_{ik}A_{kj} - \frac{1}{3}A_{pq}A_{qp}\delta_{ij}\right) - P_{ij}^{(d)} + \nu\nabla^2 A_{ij}, \tag{1}$$

where $P_{ij}^{(d)} = \partial_i\partial_j p - \frac{1}{3}\nabla^2 p\delta_{ij}$ is the deviatoric part of the pressure Hessian tensor, p is the pressure divided by density, and $\frac{d}{dt}$ represents the material time derivative following fluid particles in the flow. Treating (1) as a nine-component dynamical system (eight degrees of freedom since $A_{ii} = 0$, due to incompressibility) greatly reduces the computational effort and complexity of the Navier-Stokes system. This approach, however, requires a closure approximation for the pressure Hessian and viscous Laplacian terms [15] since these are nonlocal; they cannot be expressed in terms of the local values of A_{ij}. Nonetheless, the closed term $-A_{ik}A_{kj}$ and the isotropic effect of pressure ($\nabla^2 p = -A_{pq}A_{qp}$) in (1) contain much of the interesting physics contributing to turbulent dynamics, such as the stretching and tilting of vorticity, $\omega_i = \epsilon_{ijk}A_{kj}$, by the strain-rate tensor, $S_{ij} = \frac{1}{2}(A_{ij} + A_{ji})$ [16–18].

Various closure models have been developed, e.g., based on prescribing log normality of pseudodissipation [19], the tetrad inertia tensor evolution [20], fluid deformation approximations [21–23], and Gaussian field statistics [24,25]. So far, however, such closures have only been successful for low-to-moderate Reynolds numbers ($\mathrm{Re}_\lambda \leqslant 150$) and fail to reproduce realistic buildup of intermittency at arbitrarily high Re_λ [26]. A velocity gradient shell model [27] was a first attempt to extend this type of modeling to high Reynolds numbers, but it was based on a generic nonlinear energy-preserving intershell coupling term without clear basis in the underlying dynamical equations. Here, we propose a low-dimensional model of turbulence that can describe intermittency growth at arbitrarily high Reynolds numbers. In the following paragraph, we review the modeling approach of Ref. [25], which applies to relatively low Re_λ dynamics and provides the background for developing the new model for arbitrarily high Re_λ explained afterward.

The dynamics of (1) can be modeled by the stochastic differential equation [24],

$$dA_{ij} = \left[-\left(A_{ik}A_{kj} - \tfrac{1}{3}A_{pq}A_{qp}\delta_{ij}\right) + h_{ij}\right]dt + dF_{ij}, \tag{2}$$

where $h_{ij} = -\langle P_{ij}^{(d)}|\mathbf{A}\rangle + \nu\langle\nabla^2 A_{ij}|\mathbf{A}\rangle$ is unclosed and $dF_{ij} = b_{ijk\ell}dW_{k\ell}$ is the stochastic forcing built on the tensorial Wiener process with $\langle dW_{ij}\rangle = 0$ and $\langle dW_{ij}dW_{k\ell}\rangle = \delta_{ik}\delta_{j\ell}$. Here, boldface indicates tensor quantities and $\langle c_1|c_2\rangle$ denotes the average of c_1 conditioned on c_2. Modeling is required to specify h_{ij} and $b_{ijk\ell}$ in terms of known local quantities. The physically motivated closure we use is based on the recent deformation of Gaussian fields (RDGF) approach [25] for representing the conditional averages of the pressure Hessian and viscous Laplacian needed for h_{ij} in (2). The model assumes that pressure p and $\mathbf{A}$ are slowly varying along Lagrangian fluid trajectories (i.e., constant for a short time τ) while their spatial gradients (Hessians and Laplacian) can be related to the deformation of the surrounding fluid, itself determined by the velocity gradient tensor. Further, Gaussian field statistics are assumed for the initial ensemble on which the deformation during a short time τ is performed. With these assumptions, the conditional averages can be evaluated analytically, resulting in expressions which depend only on the deformation time scale τ and the dissipation time scale τ_K. Furthermore, prescribing the stochastic forcing dF_{ij} requires specification of two diffusion coefficients D_s and D_a, for the symmetric and antisymmetric parts, respectively. Three basic constraints are enforced. The first is the consistency of the model, requiring $\langle|S|^2\rangle = \tau_K^{-2}$ (where $|S|^2 = 2S_{ij}S_{ij}$). Also, homogeneous turbulence must satisfy $\langle Q\rangle = 0$ and $\langle R\rangle = 0$ [28] (where $Q = -\frac{1}{2}\mathrm{tr}\mathbf{A}^2$ and $R = -\frac{1}{3}\mathrm{tr}\mathbf{A}^3$). These conditions determine the three parameters (found numerically) as follows: $\tau = 0.1302\tau_K$, $D_s = 0.1014\tau_K^{-3}$, and $D_a = 0.0505\tau_K^{-3}$. More details on this model (that works well for moderate Re_λ) can be found in Ref. [25] and the Supplementary Material [29].

To reach higher Re_λ, we interpret the results of the RDGF model described above as if it represented a filtered velocity gradient $\langle A\rangle_{\mathrm{filt}} = \widetilde{A}$ at a higher Reynolds number ($\langle..\rangle_{\mathrm{filt}}$ and the tilde denote spatial filtering at some length scale that need not now be specified). The similarity between velocity gradients at a low Re_λ and filtered gradients at a larger Re_λ can be motivated by considering the gradient of the filtered Navier-Stokes equations,

$$\frac{\widetilde{d}}{dt}\widetilde{A}_{ij} = -\left(\widetilde{A}_{ik}\widetilde{A}_{kj} - \frac{1}{3}\widetilde{A}_{pq}\widetilde{A}_{qp}\delta_{ij}\right) - \widetilde{P}_{ij}^{(d)} + \nu\nabla^2\widetilde{A}_{ij} - \Sigma_{ij},$$

where $\Sigma_{ij} = \partial_j\partial_k\sigma_{ik}$ represents the effect of the subscale stress $\sigma_{ik} = \widetilde{u_i u_k} - \widetilde{u}_i\widetilde{u}_k$ typically modeled in large-eddy simulations and $\frac{\widetilde{d}}{dt}$ represents rate of change along trajectories following the coarse-grained velocity field. With a constant eddy viscosity model for the subscale stresses, the filtered gradient dynamics reduce to (1) with an enhanced viscosity. Similar modeling steps lead to the original RDGF model but for coarse-grained velocity gradients and with a (larger) time scale $\beta\tau_K$, where $\beta = \sqrt{\langle|S|^2\rangle/\langle|\widetilde{S}|^2\rangle} \gg 1$ is a model parameter specifying the extent of the coarse graining. In other words, at the large scales one solves Eq. (2) but the model uses as time scale $\tau_1 = \beta\tau_K$.

This model for $\widetilde{A}_{ij}$ provides crucial information for modeling the unfiltered velocity gradient tensor at high Re_λ, namely, the local rate at which energy is passed to smaller scales, $\Pi = -\sigma_{ij}\widetilde{S}_{ij} \approx \nu_e|\widetilde{S}|^2$, where ν_e is the effective eddy viscosity for the filtered dynamics. The rate Π must be matched by the locally averaged rate at which energy is dissipated by the unfiltered velocity gradients within a region of scale comparable to the filter scale, i.e., $\nu_e|\widetilde{S}|^2 = \widetilde{\epsilon} = \nu\langle|S|^2\rangle_{\mathrm{filt}}$. Matching these rates for each trajectory and assuming a constant ν_e leads to $\langle|S|^2\rangle_{\mathrm{filt}} = (\nu_e/\nu)|\widetilde{S}|^2$. This step shows that the local variance of the inverse time scale of the small-scale motions is slaved locally to that of the larger scale motions. Thus, the characteristic time scale for the small scales should not be a single constant value, τ_K, but should be modulated by the characteristic time scales of the larger scale motions. Specifically, a fluctuating time scale $\tau_2(t) = \beta^{-1}|\widetilde{S}|^{-1}$ should be used for the full velocity gradient dynamics (1). Therefore, the time-dependent $\tau_2(t)$ replaces the constant τ_K in the RDGF closure for the unfiltered dynamics (2) for this two-time scale model. Here, β is a fixed ratio of time scales, which can be thought of as ensuring global balance of energy dissipation rates if β^2 is interpreted as a chosen ratio of viscosities between the scales. Consistency with the model's weak coupling of small-scale $\mathbf{A}$ with coarse-grained $\widetilde{\mathbf{A}}$ requires $\beta \gg 1$, i.e., a large separation between time scales.

To reach even higher values of Re_λ, this second level ($n = 2$) can itself be thought of as a coarse-grained velocity gradient with the introduction of a third level evolving at even smaller and faster scales still to be described. In this way, the procedure outlined above can be iterated an arbitrary number of times to construct a multiple-time-scale model with N levels and $\mathrm{Re}_\lambda \approx \mathrm{Re}_{\lambda,0}\beta^{N-1}$, where $\mathrm{Re}_{\lambda,0}$ represents the effective Reynolds number of the single-level model ($\mathrm{Re}_{\lambda,0} \approx 60$ and $\beta = 10$ will be seen to describe the data well). Therefore, the adjustable parameters β and $\mathrm{Re}_{\lambda,0}$ determine the Reynolds number represented by a given number of levels by setting how quickly the effective Reynolds number grows with each additional level. The general multiple-time-scale model thus consists of a series of 3×3 tensors $\mathbf{A}^{(n)}$ with time scales $\tau_n(t)$ for $n = 1,\ldots,N$. The first level evolves with the modeling and forcing using a constant time scale of $\tau_1 = \beta^{N-1}\tau_K \sim \beta^{-1}T$, where T is the time scale of eddies at the integral scale of turbulence. All faster levels obtain their instantaneous, trajectory-specific time scale from the next coarser level using $\tau_n(t) = \beta^{-1}|S^{(n-1)}|^{-1}$.

An additional drift term must be added to the equation to account for the fact that the single-level model was calibrated for an imposed constant time scale τ_K. Because each $n \geqslant 2$ level has a fluctuating time scale, $\tau_n(t)$, which takes the place of τ_K, we must ensure that the consistency constraint $\langle|S^{(n)}|^2\rangle = \tau_n^{-2} = \beta^{-2}|S^{(n-1)}|^2$ holds. The single-level RDGF system with constant-in-time τ_K can be written in the dimensionless form:

$$\frac{d}{dt^*}A_{ij}^* = f^*(\mathbf{A}^*), \quad \text{where } A_{ij}^* = A_{ij}\tau_K,\ dt^* = dt/\tau_K, \tag{3}$$

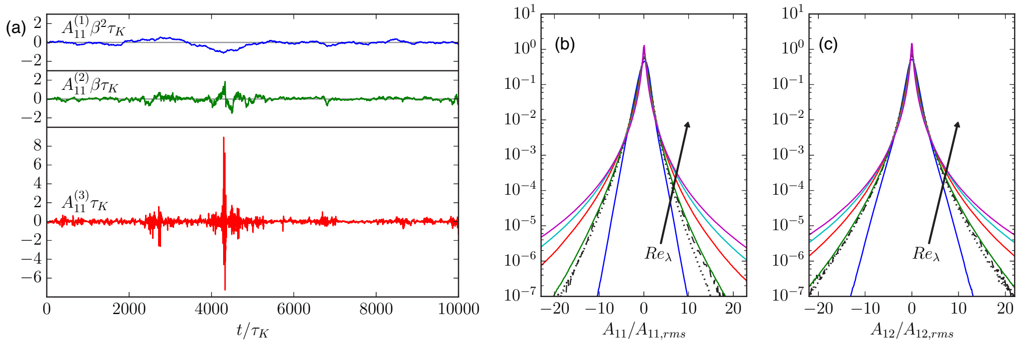

FIG. 1. (a) A sample A_{11} signal from three adjacent levels of the same trajectory in a three-level model. Top: coarsest level, $n = 1$; middle: next-coarsest level, $n = 2$. Bottom: fully resolved velocity gradient, $n = N = 3$. Panels (b) and (c): Probability density functions of A_{11} (b) and A_{12} (c) for $N = 1, 2, 3, 4$, and 5 (colored solid lines) compared with DNS data at $\mathrm{Re}_\lambda = 430$ (dotted line). Also shown is a model with $N_{\mathrm{eff}} = 1.85$ (dashed line).

and

$$f^*(\mathbf{A}^*) = -\left(A^*_{ik}A^*_{kj} - \tfrac{1}{3}A^*_{k\ell}A^*_{\ell k}\right) + h^*_{ij}(\mathbf{A}^*) + dF^*_{ij}/dt^*. \tag{4}$$

This dimensionless system satisfies $\langle |S^*|^2\rangle = 1$ by design. By replacing τ_K with $\tau_n(t)$, using the product rule to expand $\frac{d}{dt^*}(A^*_{ij}) = \tau_n \frac{d}{dt}(A_{ij}\tau_n) = \tau_n^2 \frac{d}{dt}A_{ij} + A_{ij}\tau_n \frac{d\tau_n}{dt}$, and substituting for the time derivatives, it is straightforward to obtain

$$f(\mathbf{A},\tau_n) = \frac{1}{\tau_n^2} f^*(\mathbf{A}^*) - \frac{1}{\tau_n}\frac{d\tau_n}{dt}\mathbf{A}. \tag{5}$$

Thus, the RDGF model follows an imposed arbitrary $\tau_n(t)$ signal by introducing the unsteady constraint term $-\frac{1}{\tau_n}\frac{d\tau_n}{dt}\mathbf{A}$ in the equation. Finally, the proposed multiple-time-scale Lagrangian RDGF model for the velocity gradient tensor reads

$$dA^{(n)}_{ij} = \left[-\left(A^{(n)}_{ik}A^{(n)}_{kj} - \frac{1}{3}A^{(n)}_{pq}A^{(n)}_{qp}\delta_{ij}\right) - \frac{1}{\tau_n}\frac{d\tau_n}{dt}A^{(n)}_{ij} + h^{(n)}_{ij}(\mathbf{A}^{(n)},\tau_n)\right]dt + dF^{(n)}_{ij}(\tau_n),$$
$$n = 1,2,3\ldots N \tag{6}$$

with $\tau_n(t) = \beta^{-1}|S^{(n-1)}|^{-1}$ for $n \geqslant 2$ and $\tau_1 = \beta^{N-1}\tau_K$. The full expressions for $h^{(n)}_{ij}$ and $dF^{(n)}_{ij}$ can be found in the Supplementary Material [29] and are based on the single-time-scale model of Ref. [25]. Equation (6) is a system of stochastic differential equations, representing the dynamics of coarse-grained ($1 \leqslant n < N$) and fully resolved ($n = N$) velocity gradients, with only $9N$ components yet having its roots in the Navier-Stokes dynamics.

For the numerical results shown in the paper, the stochastic differential equations are advanced numerically for 10^4 Kolmogorov times using a second-order predictor-corrector method with adaptive time step set by a tolerance of 10^{-3} relative difference between first- and second-order schemes at each time step. Each level of each trajectory is advanced with its own unique time step size. Linear temporal interpolation and central differencing in time was used to compute $\tau_n(t)$ and $d\tau_n/dt$ information passed between levels, respectively.

We begin by showing results from a three-level simulation with $\beta = 10$. Figure 1(a) shows sample time signals for $A^{(n)}_{11}$ for $n = 1,2,3$. This tensor component is the longitudinal gradient $\partial u/\partial x$ commonly studied experimentally. The coarse-grained velocity gradients vary on longer time scales and act to modulate the amplitude of the finer scale ones which change rapidly. This generates more extreme events in the faster levels. Next, we evaluate statistical and scaling properties of the

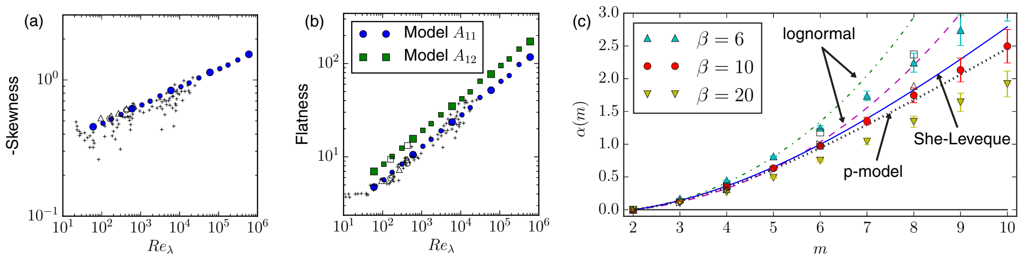

FIG. 2. Panels (a) and (b): Skewness (a) and flatness (b) factors of velocity gradient components as a function of Re_λ compared with DNS and experimental data. Filled circles (A_{11} skewness and flatness) and squares (A_{12} flatness) represent the results of the multi-level model. DNS data from Ref. [25] (□,○); Ref. [32] (△); and a compilation of experimental data from Ref. [6] (+). Smaller filled symbols represent the multilevel model with noninteger N_{eff}. (c) Scaling exponents $\alpha(m)$ from the multiple-time-scale RDGF model with ratio $\beta = 10$ (filled red circles with error bars), compared with log-normal $\mu = 0.2$ (dashed magenta line) and $\mu = 0.25$ (dot-dashed green line), She-Leveque [10] (continuous blue line), p-model [9] with $p_1 = 0.7$ (black dotted line), and DNS data from Refs. [32] (▽), [1] (△), and [33] (□), as well as experimental data from Ref. [34] (▷). The RDGF model with $\beta = 6$ and $\beta = 20$ is also shown as well, illustrating the effect of changing β on the predicted scaling exponents.

model and integrate up to $N = 5$ levels. The PDFs for A_{11} and A_{12} are shown in Figs. 1(b) and 1(c) for number of levels from $N = 1$ to $N = 5$. The distributions become increasingly heavy-tailed as more levels are added. The probability density function (PDF) from direct numerical simulation (DNS) data [30] with $\mathrm{Re}_\lambda = 430$ is also shown, with its level of intermittency falling between the results for $N = 1$ and $N = 2$.

The skewness factor of the longitudinal component, defined as $S_k = \langle A_{11}^{(N)^3}\rangle / \langle A_{11}^{(N)^2}\rangle^{3/2}$, and flatness factors $F_1 = \langle A_{11}^{(N)^4}\rangle/\rangle / \langle A_{11}^{(N)^2}\rangle^2$ (and similarly for $A_{12}^{(N)}$) of the longitudinal and transverse components are evaluated from numerical integration of the model for various N. Results are shown and compared against DNS and experimental results in Fig. 2 using $\mathrm{Re}_\lambda = 60\beta^{N-1}$, where $\beta = 10$ is chosen empirically by matching the ratio of flatness of A_{11} between the first and second levels obtained from the model to data (see first two large blue circles in Fig. 2(b)). Thus, $\mathrm{Re}_\lambda \approx 6 \times 10^5$ is reached with only 5 levels. Note that in Fig. 2(a) the negative of the skewness is shown, proving that the model predicts negative skewness consistent with the energy cascade. Values near $S_k \approx -0.5$ are obtained for moderate $\mathrm{Re}_\lambda \sim 10^2$ and rise in magnitude at higher Re_λ.

To use the model for any desired value of Re_λ in between those given by integer N, one may construct a model for a noninteger effective number of levels N_{eff}, which can be obtained by shrinking the effective ratio of time scales between the first and second levels. This is accomplished by writing $\tau_2(t)$ as a mixture with fraction γ from the fluctuations of the first level, while a fraction $1 - \gamma$ is contributed by a nonfluctuating time scale:

$$\tau_2(t) = \left[\gamma\beta^2|S^{(1)}|^2 + (1-\gamma)\beta^{-2(N-2)}\tau_K^{-2}\right]^{-1/2}. \tag{7}$$

Note that this mixing of time scales is only done between the first and second levels, while subsequent levels proceed as normal with $\tau_n(t) = \beta^{-1}|S^{(n-1)}|^{-1}$ for $n = 3, \ldots, N$. To relate the mixture fraction $0 < \gamma \leqslant 1$ to N_{eff}, we have found the following scaling to work well: $\gamma = [N_{\mathrm{eff}} - (N-1)]^{2/3}$. Thus, for a given Re_λ, one may obtain an effective (noninteger) number of levels $N_{\mathrm{eff}} = 1 + \log_\beta(\mathrm{Re}_\lambda/60)$. Then, using $\lceil N_{\mathrm{eff}} \rceil$ levels ($\lceil \cdots \rceil$ is the ceiling function), one can effectively shrink the time-scale ratio between the first and second levels. The appropriateness of this correspondence between Reynolds number and levels in the multiple-time-scale description is verified by running the model for a desired $\mathrm{Re}_\lambda = 430$ to compare with DNS. For this case, we find $N_{\mathrm{eff}} = 1 + \log_{10}(430/60) = 1.85$ and thus must choose $N = \lceil N_{\mathrm{eff}} \rceil = 2$ levels and $\gamma = 0.85^{2/3} = 0.90$. The dashed line PDF in Figs. 1(b) and 1(c) shows excellent agreement with the DNS data at that Reynolds number.

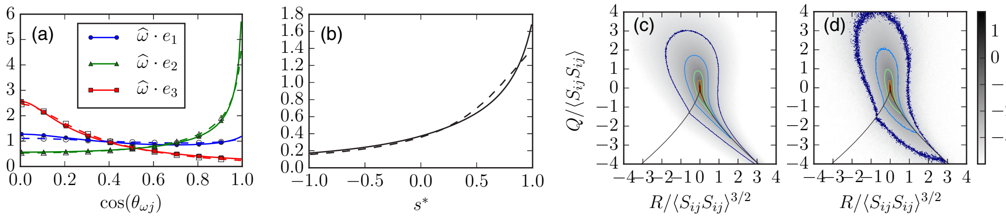

FIG. 3. Panels (a) and (b): Probability density functions of alignment of vorticity vector with the jth strain-rate eigenvector ordered by decreasing eigenvalues (a): Λ_1, circles; Λ_2, triangles; Λ_3, squares; and of s^* (b). Dashed lines indicate DNS results from Ref. [30] at $\mathrm{Re}_\lambda = 430$ and solid lines indicate model results that are the same for any N. Panels (c) and (d): Joint PDFs in RQ invariant space from the multilevel RDGF stochastic model with $\beta = 10$ and $N_{\mathrm{eff}} = 1.85$ (c) and from DNS of Ref. [30] at $\mathrm{Re}_\lambda = 430$ (d). Logarithmically spaced isocontours shown are 10^1, 10^0, 10^{-1}, 10^{-2}, and 10^{-3}.

The anomalous scaling properties of the model results can be explored via the higher order standardized moments, $\mu_m = \langle |A_{11}|^m\rangle/\langle A_{11}^2\rangle^{m/2} \sim \mathrm{Re}_\lambda^{\alpha(m)}$. These moments are evaluated from the model up to $m = 10$, yielding log-log plots with excellent scaling, as those shown in Figs. 2(a) and 2(b) (that correspond to $m = 3$ and 4, respectively). The slopes can be measured, leading to $\alpha(m)$ shown in Fig. 2(c) as filled circles. Results clearly deviate from the nonintermittent case $\alpha(m) = 0$. In order to compare with earlier cascade models, $\alpha(m)$ can be related to existing velocity increment scaling exponents, ζ_p, using Nelkin's transformation [4,31], i.e., $\alpha(m) = 2p(m) - 3m$, where $p(m)$ is the unique solution to $\zeta_p + p = 2m$. The measured $\alpha(m)$ up to $m = 10$ corresponds to about $p \approx 16$. For $\beta = 10$, the multiple-time-scale RDGF model gives similar scaling exponents as those of the She-Leveque model [10], the p-model [9], and the log-normal model with $\mu = 0.2$ for smaller m. Choosing a lower ratio of time scales, $\beta = 6$, effectively increases the intermittency in the model closer to the $\mu = 0.25$ log-normal curve for $m \leqslant 6$, although still within the variations in scaling exponents from the various DNS studies that are observed, especially at the higher moments. Increasing the ratio of time scales, e.g., $\beta = 20$, has the opposite effect in decreasing the level of intermittency. The model parameter β controls the intermittency [anomalous scaling exponents, $\alpha(m)$] in the results by changing the effective increase in Re_λ corresponding to adding one level. The increase in moments, μ_m, when adding one level is insensitive to β.

In extending the models to higher Re_λ by adding more levels, the statistical properties of local topology are maintained from the original (single-level) model. For instance, Fig. 3(a) shows the PDFs for alignment between the vorticity vector and the strain-rate eigenvectors ordered by decreasing eigenvalue, Λ_i. The vorticity's preferential alignment parallel to the intermediate strain-rate eigenvalue direction and orthogonal to the minimal eigenvalue direction is reproduced. In Fig. 3(b), the PDF of $s^* = -3\sqrt{6}\Lambda_1\Lambda_2\Lambda_3/(\Lambda_1^2 + \Lambda_2^2 + \Lambda_3^2)^{3/2}$ [35] is shown. The model produces these same PDFs for any arbitrary number of levels. Furthermore, Figs. 3(c) and 3(d) compare the joint PDF of Q and R for $N_{\mathrm{eff}} = 1.85$ with DNS at $\mathrm{Re}_\lambda = 430$. The model predicts this joint PDF well. As the number of levels increases, the outer isocontours expand as rare events become more likely, while the signature teardrop shape is maintained.

In summary, a low-dimensional model for Lagrangian time evolution of the velocity gradient tensor in fluid turbulence has been proposed. It differs fundamentally from prior shell models and other empirically motivated models of intermittency because the gradient self-stretching and rotation $\mathbf{A}^2$ term vital to the energy cascade and intermittency development is derived directly from Navier-Stokes. In this approach, each level effectively contains a wide band of dynamical frequencies ($\beta = 10$ compared to $2^{2/3}$ in Ref. [27] and typical of other shell models). The exact representation of the nonlinear term captures local-in-scale interactions naturally within each level, eliminating the need for strong, *ad hoc* coupling between levels. The model yields realistic predictions of intermittency dependence on Re_λ and describes the full tensorial structure of the velocity gradient, reflecting unique signatures and geometric alignments of velocity gradients in Navier-Stokes turbulence.

Data are publicly available through the Gulf of Mexico Research Initiative Information and Data Cooperative (GRIIDC) [36].

The authors thank M. Wilczek, L. Chevillard, L. Biferale, and F. Toschi for prior interactions leading to this work and A. Kerstein for encouraging comments, and we gratefully acknowledge their comments on this paper. P.L.J. was supported by NSF's GRFP (DGE-1232825) and C.M. was supported by a grant from The Gulf of Mexico Research Initiative.

[1] J. Schumacher, J. D. Scheel, D. Krasnov, D. A. Donzis, V. Yakhot, and K. R. Sreenivasan, Small-scale universality in fluid turbulence, PNAS **111**, 10961 (2014).
[2] A. M. Oboukhov, Some specific features of atmospheric tubulence, J. Fluid Mech. **13**, 77 (1962).
[3] A. N. Kolmogorov, A refinement of previous hypotheses concerning the local structure of turbulence in a viscous incompressible fluid at high Reynolds number, J. Fluid Mech. **13**, 82 (1962).
[4] U. Frisch, *Turbulence: The Legacy of A. N. Kolmogorov* (Cambridge University Press, New York, 1995).
[5] R. Benzi and L. Biferale, Homogeneous and isotropic turbulence: A short survey on recent developments, J. Stat. Phys. **161**, 1351 (2015).
[6] K. R. Sreenivasan and R. A. Antonia, The phenomenology of small-scale turbulence, Ann. Rev. Fluid Mech. **29**, 435 (1997).
[7] B. W. Zeff, D. D. Lanterman, R. McAllister, R. Roy, E. J. Kostelich, and D. P. Lathrop, Measuring intense rotation and dissipation in turbulent flows, Nature (London) **421**, 146 (2003).
[8] R. Benzi, G. Paladin, G. Parisi, and A. Vulpiani, On the multifractal nature of fully developed turbulence and chaotic systems, J. Phys. A **17**, 3521 (1984).
[9] C. Meneveau and K. R. Sreenivasan, Simple Multifractal Cascade Model for Fully Developed Turbulence, Phys. Rev. Lett. **59**, 1424 (1987).
[10] Z.-S. She and E. Leveque, Universal Scaling Laws in Fully Developed Turbulence, Phys. Rev. Lett. **72**, 336 (1994).
[11] L. Biferale, Shell models of energy cascade in turbulence, Ann. Rev. Fluid Mech. **35**, 441 (2003).
[12] R. Friedrich and J. Peinke, Description of a turbulent cascade by a Fokker-Planck equation, Phys. Rev. Lett. **78**, 863 (1997).
[13] K. Gawedzki and A. Kupiainen, Anomalous Scaling of the Passive Scalar, Phys. Rev. Lett. **75**, 3834 (1995).
[14] S. B. Pope, *Turbulent Flows* (Cambridge University Press, Cambridge, UK, 2000).
[15] C. Meneveau, Lagrangian dynamics and models of the velocity gradient tensor in turbulent flows, Ann. Rev. Fluid Mech. **43**, 219 (2011).
[16] P. Vieillefosse, Local interaction between vorticity and shear in a perfect incompressible fluid, J. Phys. **43**, 837 (1982).
[17] P. Vieillefosse, Internal motion of a small element of fluid in an inviscid flow, Phys. A (Amsterdam, Neth.) **125**, 150 (1984).
[18] B. J. Cantwell, Exact solution of a restricted Euler equation for the velocity gradient tensor, Phys. Fluids **4**, 782 (1992).
[19] S. S. Girimaji and S. B. Pope, A diffusion model for velocity gradients in turbulence, Phys. Fluids **2**, 242 (1990).
[20] M. Chertkov, A. Pumir, and B. I. Shraiman, Lagrangian tetrad dynamics and the phenomenology of turbulence, Phys. Fluids **11**, 2394 (1999).
[21] E. Jeong and S. S. Girimaji, Velocity-gradient dynamics in turbulence: Effect of viscosity and forcing, Theoret. Comp. Fluid Dyn. **16**, 421 (2003).
[22] L. Chevillard and C. Meneveau, Lagrangian Dynamics and Statistical Geometric Structure of Turbulence, Phys. Rev. Lett. **97**, 174501 (2006).

[23] L. Chevillard, C. Meneveau, L. Biferale, and F. Toschi, Modeling the pressure Hessian and viscous Laplacian in turbulence: Comparisons with direct numerical simulation and implications on velocity gradient dynamics, Phys. Fluids **20**, 101504 (2008).

[24] M. Wilczek and C. Meneveau, Pressure Hessian and viscous contributions to velocity gradient statistics based on Gaussian random fields, J. Fluid Mech. **756**, 191 (2014).

[25] P. L. Johnson and C. Meneveau, A closure for Lagrangian velocity gradient evolution in turbulence using recent deformation mapping of initially Gaussian fields, J. Fluid Mech. **804**, 387 (2016).

[26] M. M. Afonso and C. Meneveau, Recent fluid deformation closure for velocity gradient tensor dynamics in turbulence: Timescale effects and expansions, Phys. D (Amsterdam, Neth.) **239**, 1241 (2010).

[27] L. Biferale, L. Chevillard, C. Meneveau, and F. Toschi, Multiscale Model of Gradient Evolution in Turbulent Flows, Phys. Rev. Lett. **98**, 214501 (2007).

[28] R. Betchov, An inequality concerning the production of vorticity in isotropic turbulence, J. Fluid Mech. **1**, 497 (1956).

[29] See Supplemental Material at http://link.aps.org/supplemental/10.1103/PhysRevFluids.2.072601 for the full mathematical details of the model described in the text.

[30] Y. Li, E. Perlman, M. Wan, Y. Yang, C. Meneveau, R. Burns, S. Chen, A. Szalay, and G. Eyink, A public turbulence database cluster and applications to study Lagrangian evolution of velocity increments in turbulence, J. Turbulence **9**, 1 (2008).

[31] M. Nelkin, Multifractal scaling of velocity derivatives in turbulence, Phys. Rev. A **42**, 7226 (1990).

[32] T. Ishihara, Y. Kaneda, M. Yokokawa, K. Itakura, and A. Uno, Small-scale statistics in high-resolution direct numerical simulation of turbulence: Reynolds number dependence of one-point velocity gradient statistics, J. Fluid Mech. **592**, 335 (2007).

[33] J. Boschung, Exact relations between the moments of dissipation and longitudinal velocity derivatives in turbulent flows, Phys. Rev. E **92**, 043013 (2015).

[34] R. A. Antonia, A. J. Chambers, and B. R. Satyaprakash, Reynolds number dependence of high-order moments of the streamwise turbulent velocity derivative, Boundary-Layer Meteorol. **21**, 159 (1981).

[35] T. S. Lund and M. M. Rogers, An improved measure of strain state probability in turbulent flows, Phys. Fluids **6**, 1838 (1994).

[36] https://data.gulfresearchinitiative.org (doi:10.7266/N76H4FVJ).